# Robust Control of a Triple Inverted Pendulum using $\mu$-Synthesis [1]

**P.Hr. Petkov**[2], **D.-W. Gu** and **M.M. Konstantinov**[3]

Control Systems Research
Department of Engineering
University of Leicester
Leicester LE1 7RH, U.K.

Email: dag@le.ac.uk

[1]This paper presents research results of the European Community BRITE-EURAM III Thematic Networks Programme NICONET (contract number BRRT-CT97-5040) and is distributed by the Working Group on Software WGS. *WGS secretariat*: Mrs. Ida Tassens, ESAT - Katholieke Universiteit Leuven, K. Mercierlaan 94, 3001-Leuven-Heverlee, BELGIUM. This report is also available by anonymous ftp from *wgs.esat.kuleuven.ac.be/pub/WGS/REPORTS/SLWN2001-1.ps.Z*

[2]Department of Automatics, Technical University of Sofia, 1756 Sofia, Bulgaria.

[3]University of Architecture & Civil Engineering, 1 Hr. Smirnenski Blv., 1421 Sofia, Bulgaria.

**Abstract**

In this paper we show the application of some of the *SLICOT* routines in the $\mu$-synthesis of a robust control system for a triple inverted pendulum. We consider the case of a mixed type uncertainty consisting of two complex uncertainties in the actuators, three real uncertainties in the moments of inertia and three real uncertainties in the viscous friction coefficients. Using the D-K iteration a $\mu$-controller is constructed for which the closed-loop control system achieves robust stability and robust performance. The influence of the individual types of uncertainties on the robust stability is investigated using $\mu$-analysis. In addition a reduced order controller is found such that the robust stability and robust performance of the closed-loop system are preserved with the much lower order controller.

**Key Words**: Robust control systems design, $\mu$-analysis and synthesis, *SLICOT*

# 1 Introduction

A triple inverted pendulum is an interesting control system which resembles many features found in walking robots and other industrial problems. The study of a triple inverted pendulum control system is of practical importance. On the other hand, this kind of pendulum systems is difficult to control due to the inherent instability and nonlinear behaviours with parametric uncertainties. Hence, it may serve as a benchmark problem for evaluating the modern design techniques as well as computational algorithms.

The control system design of triple inverted pendulum systems has been considered in several papers (see [5, 7, 8, 9]). Usually it is assumed that the system is affected by unstructured uncertainties and thus the robust properties of the closed-loop system are achieved by using a continuous-time or discrete-time $H_\infty$ controller. In practice, however, the uncertainties of such a pendulum system would be more reasonably considered to have some structures. For instance, because the moments of inertia and the friction coefficients are difficult to be estimated precisely, it makes sense to assume unknown deviations on those parameters. Also, we would like to design the closed loop control system more "robust"against those parameters which have "bigger"or more serious influence upon the system behaviour. For instance, the viscous friction in the joints may destroy the controllability of the linearized model. Hence it would be important to treat uncertainties on such parameters individually rather mixed them in an overall system dynamic, unstructured uncertainty. It is, therefore, apparent that in the triple inverted pendulum control system design it is much more suitable to apply the $\mu$-synthesis technique which may lead to a less conservative design to meet tighter design specifications.

Another major objective of this work is to test the relevant routines developed in the *SLICOT* package. In the pendulum control system design we consider a mixed type uncertainty consisting of two complex uncertainties in the actuators, three real uncertainties in the moments of inertia and three real uncertainties in the viscous friction coefficients. Hence, it is hoped that the *SLICOT* routine `AB13MD` can, which calculates the $\mu$ values and is implemented in the mex-file `mucomp`, be fully tested. The design of the $\mu$ controller follows the D-K iteration procedure. In the evaluation of the design, the influence of the individual uncertainties on the robust stability is investigated, in addition to the overall system's robust stability and robust performance. The $\mu$ controller designed is initially of high order, which is not that suitable in the practical implementation. A model reduction is thus considered. Another *SLICOT* mex-file `sysred` is used to generate a reduced order controller which preserves the required robust stability and robust performance of the closed-loop system.

## 2 Description of the triple inverted pendulum

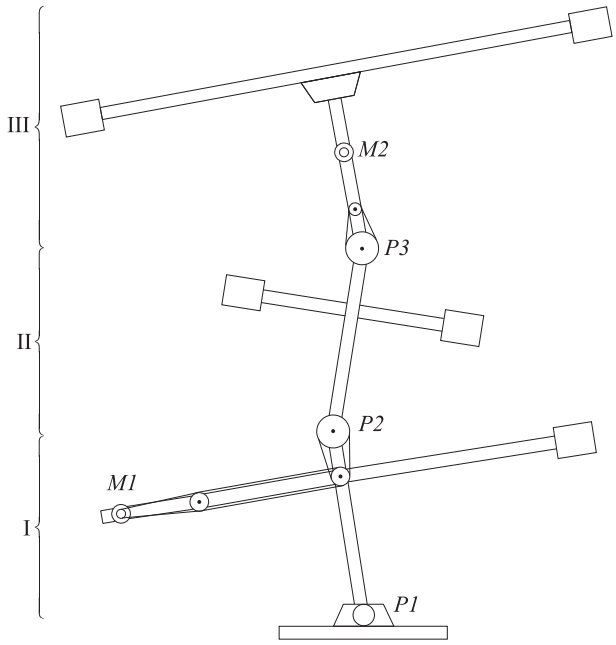


Figure 1: Triple inverted pendulum

The triple inverted pendulum is considered in the form of the experimental setup realised by Furuta, Ochiai and Ono [5] (Figure 1). The pendulum consists of three arms which are hinged by ball bearings and can rotate in the vertical plane. The torques of two upper hinges are controlled with the lowest hinge made free for rotation. By controlling the angles of the two upper arms around the specified values, the pendulum can be stabilized inversely with the desired angle attitudes. A horizontal bar is fixed to each of the arms to ease the control by increasing the moment of inertia. Two DC motors, $M_1$ and $M_2$, are mounted on the first and third arm, respectively, acting as actuators which provide torques to the two upper hinges through timing belts. The potentiometers $P_1$, $P_2$ and $P_3$ are fixed to the hinges to measure the corresponding angles. Let $\Theta_i$ denotes the angle of the $i$-th arm. The first potentiometer measures the angle $\Theta_1$, and the second and third potentiometers measure the angles $\Theta_2 - \Theta_1$ and $\Theta_3 - \Theta_2$, respectively (Figure 2).

The mathematical description of the triple inverted pendulum is derived under the following assumptions:

a) each arm is a rigid body;

b) the lengths of the belts remain constant during the work of the system;

c) the friction force in the bottom hinge is proportional to the velocity of the bottom arm and

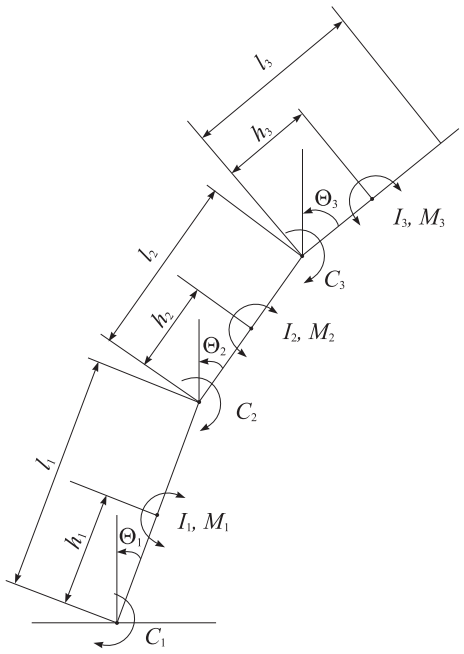


Figure 2: Geometric relationships for the triple inverted pendulum

the friction forces in the upper hinges are proportional to the differences of the respective velocities of two neighbouring arms.

First we shall consider the mathematical description of the pendulum itself without the actuators. The pendulum model is constructed using the Lagrange differential equations [5]. After linearization of these equations under the assumption of small deviations of the pendulum from the vertical position one obtains the vector-matrix equation

$$M \begin{bmatrix} \ddot{\Theta}_1 \\ \ddot{\Theta}_2 \\ \ddot{\Theta}_3 \end{bmatrix} + N \begin{bmatrix} \dot{\Theta}_1 \\ \dot{\Theta}_2 \\ \dot{\Theta}_3 \end{bmatrix} + P \begin{bmatrix} \Theta_1 \\ \Theta_2 \\ \Theta_3 \end{bmatrix} + G \begin{bmatrix} t_{m_1} \\ t_{m_2} \end{bmatrix} = 0, \tag{2.1}$$

where

$$M = \begin{bmatrix} J_1 + I_{p_1} & l_1 M_2 - I_{p_1} & l_1 M_3 \\ l_1 M_2 - I_{p_1} & J_2 + I_{p_1} + I_{p_2} & l_2 M_3 - I_{p_2} \\ l_1 M_3 & l_2 M_3 - I_{p_2} & J_3 + I_{p_2} \end{bmatrix},$$

$$N = \begin{bmatrix} C_1 + C_2 + C_{p_1} & -C_2 - C_{p_1} & 0 \\ -C_2 - C_{p_1} & C_{p_1} + C_{p_2} + C_2 + C_3 & -C_3 - C_{p_2} \\ 0 & -C_3 - C_{p_2} & C_3 + C_{p_2} \end{bmatrix},$$

Table 1: System nomenclature

| Symbol | Description |
|---|---|
| $u_j$ | input voltage to the $j$-th motor |
| $t_{m_j}$ | control torque of the $j$-th motor |
| $l_i$ | length of the $i$-th arm |
| $h_i$ | the distance from the bottom to the center of gravity of $i$-th arm |
| $m_i$ | mass of the $i$-th arm |
| $I_i$ | moment of inertia of $i$-th arm around the center of gravity |
| $C_i$ | coefficient of viscous friction of $i$-th hinge |
| $\Theta_i$ | angle of $i$-th arm from vertical line |
| $C_{m_i}$ | coefficient of viscous friction of $i$-th motor |
| $I_{m_i}$ | moment of inertia of $i$-th motor |
| $K_i$ | ratio of teeth of belt-pulley system of $i$-th hinge |
| $C_{p_i'}$ | coefficient of viscous friction of belt-pulley system of $i$-th hinge |
| $I_{p_i'}$ | moment of inertia of belt-pulley system of $i$-th hinge |
| $\alpha_i$ | gain of the $i$-th potentiometer |
| $g$ | acceleration of gravity |

$$P = \begin{bmatrix} M_1 g & 0 & 0 \\ 0 & -M_2 g & 0 \\ 0 & 0 & -M_3 g \end{bmatrix}, \; G = \begin{bmatrix} K_1 & 0 \\ -K_1 & K_2 \\ 0 & -K_2 \end{bmatrix},$$

$$C_{p_i} = C_{p_i'} + K_i^2 C_{m_i}, \; I_{p_i} = I_{p_i'} + K_i^2 I_{m_i},$$

$$M_1 = m_1 h_1 + m_2 l_1 + m_3 l_1, \; M_2 = m_2 h_2 + m_3 l_2, \; M_3 = m_3 h_3,$$

$$J_1 = I_1 + m_1 h_1^2 + m_2 l_1^2 + m_3 l_1^2, \; J_2 = I_2 + m_2 h_2^2 + m_3 l_2^2,$$

$$J_3 = I_3 + m_3 h_3^2$$

and all the other parameters and variables are defined in Table 1.

Table 2: Nominal values of the parameters

| Symbol | Value | Symbol | Value |
|---|---|---|---|
| $l_1$ (m) | 0.5 | $\alpha_1$ (1/rad) | 1.146 |
| $l_2$ (m) | 0.4 | $\alpha_2$ (1/rad) | 1.146 |
| $h_1$ (m) | 0.35 | $\alpha_3$ (1/rad) | 0.9964 |
| $h_2$ (m) | 0.181 | $C_{m_1}$ (Nms) | $2.19 \times 10^{-3}$ |
| $h_3$ (m) | 0.245 | $C_{m_2}$ (Nms) | $7.17 \times 10^{-4}$ |
| $m_1$ (kg) | 3.25 | $I_{m_1}$ (kgm$^2$) | $2.40 \times 10^{-5}$ |
| $m_2$ (kg) | 1.90 | $I_{m_2}$ (kgm$^2$) | $4.90 \times 10^{-6}$ |
| $m_3$ (kg) | 2.23 | $C_{p_1'}$ (Nms) | 0 |
| $I_1$ (kgm$^2$) | 0.654 | $C_{p_2'}$ (Nms) | 0 |
| $I_2$ (kgm$^2$) | 0.117 | $I_{p_1'}$ (kgm$^2$) | $7.95 \times 10^{-3}$ |
| $I_3$ (kgm$^2$) | 0.535 | $I_{p_2'}$ (kgm$^2$) | $3.97 \times 10^{-3}$ |
| $C_1$ (Nms) | $6.54 \times 10^{-2}$ | $K_1$ | 30.72 |
| $C_2$ (Nms) | $2.32 \times 10^{-2}$ | $K_2$ | 27.00 |
| $C_3$ (Nms) | $8.80 \times 10^{-3}$ | | |

By introducing the control torques vector $t_m = [t_{m_1}\ t_{m_2}]^T$ and denoting $\Theta = [\Theta_1\ \Theta_2\ \Theta_3]^T$, the equation (2.1) can be written in the form

$$M\ddot{\Theta} + N\dot{\Theta} + P\Theta + Gt_m = 0.$$

i.e.

$$\ddot{\Theta} = -M^{-1}N\dot{\Theta} - M^{-1}P\Theta - M^{-1}Gt_m.$$

The nominal values of the parameters are given in Table 2.

## 3 Modelling of the uncertainties

Based on practical considerations, we in particular consider the variations of the moments of inertia $I_1$, $I_2$ and $I_3$ of the three arms and the variations of the viscous friction coefficients $C_1$, $C_2$, $C_3$ and $C_{p_1}$, $C_{p_2}$. It is assumed, that the moments of inertia are constants but with possible relative error of 15% around the nominal values; similarly, the friction coefficients are with 20% relative errors.

Notice that in the rest of the report, a parameter with a bar above denotes its nominal value. Therefore, the actual moments of inertia are presented as

$$I_i = \bar{I}_i(1 + p_i\delta_{I_i}),\ i = 1,\ 2,\ 3,$$

where $\bar{I}_i$ is the nominal value of the corresponding moment of inertia, $p_i = 0.15$ is the maximum relative uncertainty in each of these moments and $-1 \leq \delta_{I_i} \leq 1,\ i = 1,\ 2,\ 3$. As a result the matrix $M$ is obtained in the form

$$M = \bar{M} + M_p\Delta_I,$$

where the elements of $\bar{M}$ are determined by the nominal values of the moments of inertia,

$$\bar{M} = \begin{bmatrix} \bar{J}_1 + \bar{I}_{p_1} & \bar{l}_1\bar{M}_2 - \bar{I}_{p_1} & \bar{l}_1\bar{M}_3 \\ \bar{l}_1\bar{M}_2 - \bar{I}_{p_1} & \bar{J}_2 + \bar{I}_{p_1} + \bar{I}_{p_2} & \bar{l}_2\bar{M}_3 - \bar{I}_{p_2} \\ \bar{l}_1\bar{M}_3 & \bar{l}_2\bar{M}_3 - \bar{I}_{p_2} & \bar{J}_3 + \bar{I}_{p_2} \end{bmatrix},$$

and

$$M_p = \begin{bmatrix} \bar{I}_1 p_1 & 0 & 0 \\ 0 & \bar{I}_2 p_2 & 0 \\ 0 & 0 & \bar{I}_3 p_3 \end{bmatrix}, \Delta_I = \begin{bmatrix} \delta_{I_1} & 0 & 0 \\ 0 & \delta_{I_2} & 0 \\ 0 & 0 & \delta_{I_3} \end{bmatrix}.$$

Next we will need the matrix $M^{-1}$. Using the Matrix Inversion Lemma we obtain

$$M^{-1} = \bar{M}^{-1} - \bar{M}^{-1}M_p\Delta_I(I_3 + \bar{M}^{-1}M_p\Delta_I)^{-1}\bar{M}^{-1}$$

where $I_3$ is the $3 \times 3$ unit matrix.The matrix $M^{-1}$ can be represented as an upper Linear Fractional Transformation (LFT)

$$M^{-1} = F_U(Q_I, \Delta_I) = Q_{I_{22}} + Q_{I_{21}}\Delta_I(I_3 - Q_{I_{11}}\Delta_I)^{-1}Q_{I_{12}}$$

where

$$Q_{I_{11}} = -\bar{M}^{-1}M_p,\ Q_{I_{12}} = \bar{M}^{-1},$$

$$Q_{I_{21}} = -\bar{M}^{-1}M_p,\ Q_{I_{22}} = \bar{M}^{-1},$$

such that

$$Q_I = \begin{bmatrix} Q_{I_{11}} & Q_{I_{12}} \\ Q_{I_{21}} & Q_{I_{22}} \end{bmatrix} = \begin{bmatrix} -\bar{M}^{-1}M_p & \bar{M}^{-1} \\ -\bar{M}^{-1}M_p & \bar{M}^{-1} \end{bmatrix}.$$

Let us now consider the uncertainties in the friction coefficients. It can be seen that $C_{p_1}$ and $C_{p_2}$ always appear together with $C_2$ and $C_3$ in the elements of the matrix $N$, and the magnitude of $C_{p_1}$

and $C_{p_2}$ is much smaller in comparison to that of $C_2$ and $C_3$ and, hence, the uncertainties in them have less influence in the system dynamics. We may assume

$$C_2 + C_{p_1} = (\bar{C}_2 + \bar{C}_{p_1})(1 + s_2\delta_{C_2}),$$

$$C_3 + C_{p_2} = (\bar{C}_3 + \bar{C}_{p_2})(1 + s_3\delta_{C_3}),$$

where $s_2 = 0.2,\ s_3 = 0.2$ and $-1 \leq \delta_{C_2} \leq 1,\ -1 \leq \delta_{C_3} \leq 1$. Also we set

$$C_1 = \bar{C}_1(1 + s_1\delta_{C_1}),$$

where $s_1 = 0.2$ and $-1 \leq \delta_{C_1} \leq 1$.

Taking into account the uncertainties in the friction coefficients we obtain

$$N = \bar{N} + \Delta N$$

where

$$\bar{N} = \begin{bmatrix} \bar{C}_1 + \bar{C}_2 + \bar{C}_{p_1} & -\bar{C}_2 - \bar{C}_{p_1} & 0 \\ -\bar{C}_2 - \bar{C}_{p_1} & \bar{C}_2 + \bar{C}_{p_1} + \bar{C}_3 + \bar{C}_{p_2} & -\bar{C}_3 - \bar{C}_{p_2} \\ 0 & -\bar{C}_3 - \bar{C}_{p_2} & \bar{C}_3 + \bar{C}_{p_2} \end{bmatrix}$$

and

$$\Delta N = \begin{bmatrix} \bar{C}_1 s_1\delta_{C_1} + (\bar{C}_2 + \bar{C}_{p_1})s_2\delta_{C_2} & -(\bar{C}_2 + \bar{C}_{p_1})s_2\delta_{C_2} & 0 \\ -(\bar{C}_2 + \bar{C}_{p_1})s_2\delta_{C_2} & (\bar{C}_2 + \bar{C}_{p_1})s_2\delta_{C_2} & -(\bar{C}_3 + \bar{C}_{p_2})s_3\delta_{C_3} \\ & +(\bar{C}_3 + \bar{C}_{p_2})s_3\delta_{C_3} & \\ 0 & -(\bar{C}_3 + \bar{C}_{p_2})s_3\delta_{C_3} & (\bar{C}_3 + \bar{C}_{p_2})s_3\delta_{C_3} \end{bmatrix}$$

The matrix $\Delta N$ may be represented as

$$\Delta N = N_1\Delta_C N_2$$

where

$$N_1 = \begin{bmatrix} \bar{C}_1 s_1 & -(\bar{C}_2 + \bar{C}_{p_1})s_2 & 0 \\ 0 & (\bar{C}_2 + \bar{C}_{p_1})s_2 & -(\bar{C}_3 + \bar{C}_{p_2})s_3 \\ 0 & 0 & (\bar{C}_3 + \bar{C}_{p_2})s_3 \end{bmatrix},$$

$$N_2 = \begin{bmatrix} 1 & 0 & 0 \\ -1 & 1 & 0 \\ 0 & -1 & 1 \end{bmatrix},\ \Delta_C = \begin{bmatrix} \delta_{C_1} & 0 & 0 \\ 0 & \delta_{C_2} & 0 \\ 0 & 0 & \delta_{C_3} \end{bmatrix}.$$

The matrix $N = \bar{N} + N_1\Delta_C N_2$ may be represented as an upper LFT

$$N = F_U(Q_C, \Delta_C) = Q_{C_{22}} + Q_{C_{21}}\Delta_C(I_3 - Q_{C_{11}}\Delta_C)^{-1}Q_{C_{12}}$$

where

$$Q_{C_{11}} = 0_{3\times 3},\ Q_{C_{12}} = N_2,\ Q_{C_{21}} = N_1,\ Q_{C_{22}} = \bar{N}.$$

such that

$$Q_C = \begin{bmatrix} Q_{C_{11}} & Q_{C_{12}} \\ Q_{C_{21}} & Q_{C_{22}} \end{bmatrix} = \begin{bmatrix} 0_{3\times 3} & N_2 \\ N_1 & \bar{N} \end{bmatrix}.$$

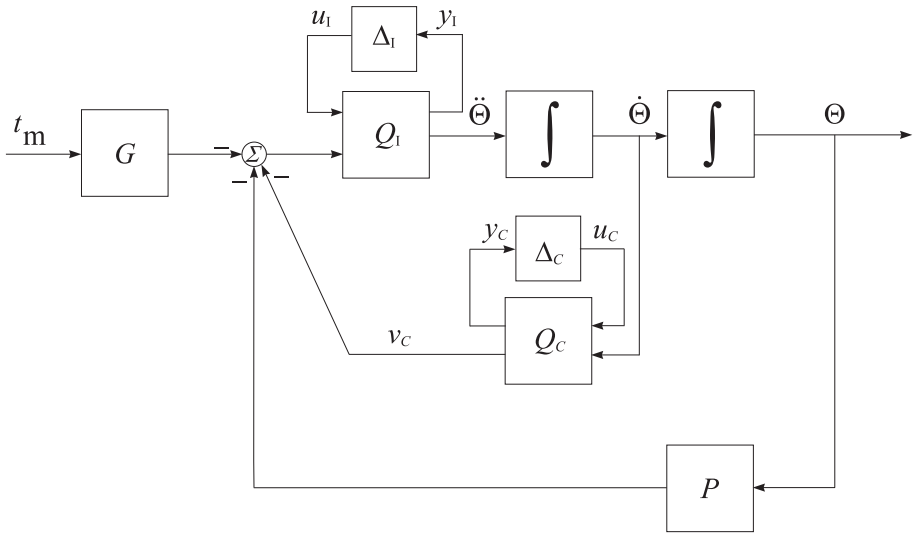


Figure 3: Block diagram of the triple inverted pendulum with uncertain parameters

To represent the pendulum model as an LFT of the real uncertain parameters $\delta_{I_1},\ \delta_{I_2},\ \delta_{I_3},\ \delta_{C_1},\ \delta_{C_2}$ and $\delta_{C_3}$, we shall isolate first the uncertain parameters and denote the inputs and outputs of $\Delta_I$ and $\Delta_C$ as $y_I,\ y_C$ and $u_I,\ u_C$, respectively, as shown in Figure 3. The pendulum equations are written then as

$$\begin{aligned}
\begin{bmatrix} y_I \\ \ddot{\Theta} \end{bmatrix} &= \begin{bmatrix} -\bar{M}^{-1}M_p & \bar{M}^{-1} \\ -\bar{M}^{-1}M_p & \bar{M}^{-1} \end{bmatrix} \begin{bmatrix} u_I \\ -(Gt_m + v_C + P\Theta) \end{bmatrix}, \\
\begin{bmatrix} y_c \\ v_c \end{bmatrix} &= \begin{bmatrix} 0_{3\times 3} & N_2 \\ N_1 & \bar{N} \end{bmatrix} \begin{bmatrix} u_c \\ \dot{\Theta} \end{bmatrix}, \\
u_I &= \Delta_I y_I, \\
u_C &= \Delta_C y_C.
\end{aligned}$$

The pendulum state vector

$$x = [x_1\ x_2\ x_3\ x_4\ x_5\ x_6]^T,$$

is chosen such that

$$x_1 = \Theta_1,\ x_2 = \Theta_2,\ x_3 = \Theta_3,\ x_4 = \dot{\Theta}_1,\ x_5 = \dot{\Theta}_2,\ x_6 = \dot{\Theta}_3.$$

Hence

$$\left[\ \dot{x}_1\ \dot{x}_2\ \dot{x}_3\ \right]^T = \dot{\Theta}$$

and

$$\left[\ \dot{x}_4\ \dot{x}_5\ \dot{x}_6\ \right]^T = \ddot{\Theta}.$$

As an output vector we take

$$y = [\Theta_1\ \Theta_2\ \Theta_3]^T.$$

The outputs are measured by linear potentiometers, whose voltages are given by

$$y_{p_1} = \alpha_1\Theta_1,\ y_{p_2} = \alpha_2(\Theta_2 - \Theta_1),\ y_{p_3} = \alpha_3(\Theta_3 - \Theta_2).$$

Introducing the vector of the measured outputs

$$y_p = [y_{p_1}\ y_{p_2}\ y_{p_3}]^T$$

we obtain that

$$y_p = C_p\Theta,\ \ C_p = \begin{bmatrix} \alpha_1 & 0 & 0 \\ -\alpha_2 & \alpha_2 & 0 \\ 0 & -\alpha_3 & \alpha_3 \end{bmatrix}.$$

As a result we obtain the system of equations

$$\begin{aligned}
\begin{bmatrix} \dot{x}_1 \\ \dot{x}_2 \\ \dot{x}_3 \end{bmatrix} &= \dot{\Theta}, \\
\begin{bmatrix} \dot{x}_4 \\ \dot{x}_5 \\ \dot{x}_6 \end{bmatrix} &= -\bar{M}^{-1}M_p u_I - \bar{M}^{-1}(Gt_m + v_C + P\Theta), \\
y_I &= -\bar{M}^{-1}M_p u_I - \bar{M}^{-1}(Gt_m + v_C + P\Theta), \\
y_C &= N_2\dot{\Theta}, \\
v_C &= N_1 u_C + \bar{N}\dot{\Theta}, \\
y &= \Theta, \\
y_p &= C_p\Theta, \\
u_I &= \Delta_I y_I, \\
u_C &= \Delta_C y_C.
\end{aligned}$$

Excluding the variable $v_C$ this system of equations is represented as

$$\left[\begin{array}{c} \dot{x}_1 \\ \dot{x}_2 \\ \dot{x}_3 \\ \dot{x}_4 \\ \dot{x}_5 \\ \dot{x}_6 \\ -- \\ y_I \\ y_C \\ -- \\ y \\ y_p \end{array}\right] = \left[\begin{array}{ccc|ccc} & & & & & \\ 0_{3\times3} & I_{3\times3} & 0_{3\times3} & 0_{3\times3} & 0_{3\times2} \\ & & & & & \\ & & & & & \\ -\bar{M}^{-1}P & -\bar{M}^{-1}\bar{N} & -\bar{M}^{-1}M_p & -\bar{M}^{-1}N_1 & -\bar{M}^{-1}G \\ & & & & & \\ \hline -\bar{M}^{-1}P & -\bar{M}^{-1}\bar{N} & -\bar{M}^{-1}M_p & -\bar{M}^{-1}N_1 & -\bar{M}^{-1}G \\ 0_{3\times3} & N_2 & 0_{3\times3} & 0_{3\times3} & 0_{3\times2} \\ \hline I_{3\times3} & 0_{3\times3} & 0_{3\times3} & 0_{3\times3} & 0_{3\times2} \\ C_p & 0_{3\times3} & 0_{3\times3} & 0_{3\times3} & 0_{3\times2} \end{array}\right] \left[\begin{array}{c} x_1 \\ x_2 \\ x_3 \\ x_4 \\ x_5 \\ x_6 \\ -- \\ u_I \\ u_C \\ -- \\ t_m \end{array}\right], \tag{3.2}$$

$$\left[\begin{array}{c} u_I \\ u_C \end{array}\right] = \left[\begin{array}{cc} \Delta_I & 0 \\ 0 & \Delta_C \end{array}\right] \left[\begin{array}{c} y_I \\ y_C \end{array}\right]. \tag{3.3}$$

In this way the pendulum model

$$\left[\begin{array}{c} y_I \\ y_C \\ y \\ y_p \end{array}\right] = G_{pend} \left[\begin{array}{c} u_I \\ u_C \\ t_m \end{array}\right]$$

is an eight input, twelve output system with six states, where

$$G_{pend} = \left[\begin{array}{c|cc} A & B_1 & B_2 \\ \hline C_1 & D_{11} & D_{12} \\ C_2 & D_{21} & D_{22} \end{array}\right]$$

and

$$A = \left[\begin{array}{cc} 0_{3\times3} & I_{3\times3} \\ -\bar{M}^{-1}P & -\bar{M}^{-1}\bar{N} \end{array}\right],\ B_1 = \left[\begin{array}{cc} 0_{3\times3} & 0_{3\times3} \\ -\bar{M}^{-1}M_p & -\bar{M}^{-1}N_1 \end{array}\right],\ B_2 = \left[\begin{array}{c} 0_{3\times2} \\ -\bar{M}^{-1}G \end{array}\right],$$

$$C_1 = \left[\begin{array}{cc} -\bar{M}^{-1}P & -\bar{M}^{-1}\bar{N} \\ 0_{3\times3} & N_2 \end{array}\right],\ D_{11} = \left[\begin{array}{cc} -\bar{M}^{-1}M_p & -\bar{M}^{-1}N_1 \\ 0_{3\times3} & 0_{3\times3} \end{array}\right],\ D_{12} = \left[\begin{array}{c} -\bar{M}^{-1}G \\ 0_{3\times2} \end{array}\right],$$

$$C_2 = \left[\begin{array}{cc} I_{3\times3} & 0_{3\times3} \\ C_p & 0_{3\times3} \end{array}\right],\ D_{21} = 0_{6\times6},\ D_{22} = 0_{6\times2}.$$

The uncertain behaviour of the pendulum is described by the upper LFT

$$\left[\begin{array}{c} y \\ y_p \end{array}\right] = F_U(G_{pend}, \Delta_{pend}) t_m$$

with diagonal uncertain matrix

$$\Delta_{pend} = \begin{bmatrix} \Delta_I & 0 \\ 0 & \Delta_C \end{bmatrix}$$

Consider now the actuator models. The transfer functions of the actuators are taken as first order phase-lag models

$$G_{m_1} = \frac{K_{m_1}}{T_{m_1}s + 1}, \quad G_{m_2} = \frac{K_{m_2}}{T_{m_2}s + 1}$$

where the nominal values of the parameters are

$$\bar{K}_{m_1} = 1.08, \ \bar{T}_{m_1} = 0.005, \ \bar{K}_{m_2} = 0.335, \ \bar{T}_{m_2} = 0.002.$$

It is assumed that the gain coefficients $K_{m_1}$, $K_{m_2}$ are known with relative error 10% and the time constants $T_{m_1}$, $T_{m_2}$ - with relative error 20%. The uncertain frequency responses of the actuators are shown in Figure 4. In order to account for unmodelled dynamics and nonlinear effects, the uncertainties in the actuator

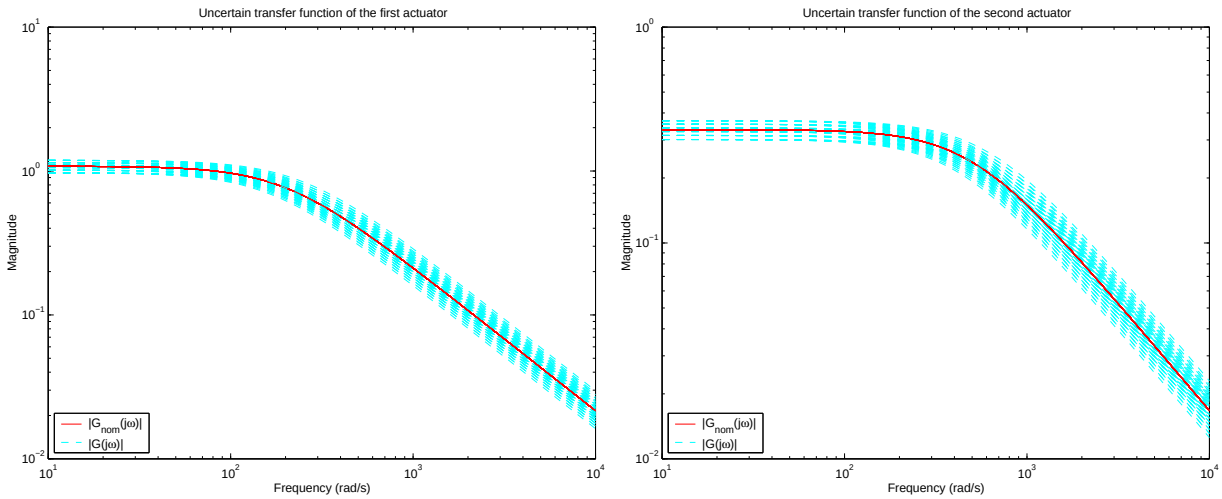


Figure 4: Uncertain frequency responses of the actuators

models are approximated by input multiplicative uncertainties which gives rise to the perturbed transfer functions

$$\tilde{G}_{m_1} = (1 + W_{m_1}\delta_{m_1})G_{m_1}, \quad \tilde{G}_{m_2} = (1 + W_{m_2}\delta_{m_2})G_{m_2}$$

where

$$|\delta_{m_1}| \leq 1, \quad |\delta_{m_2}| \leq 1$$

and the uncertainty weights $W_{m_1}$, $W_{m_2}$ are chosen so that

$$\frac{\left|\tilde{G}_{m_1}(j\omega) - G_{m_1}(j\omega)\right|}{|G_{m_1}(j\omega)|} < |W_{m_1}(j\omega)|, \quad \frac{\left|\tilde{G}_{m_2}(j\omega) - G_{m_2}(j\omega)\right|}{|G_{m_2}(j\omega)|} < |W_{m_2}(j\omega)|.$$

The frequency responses of $W_{m_1}$, $W_{m_2}$ are found graphicaly as shown in Figure 5 and then approximated

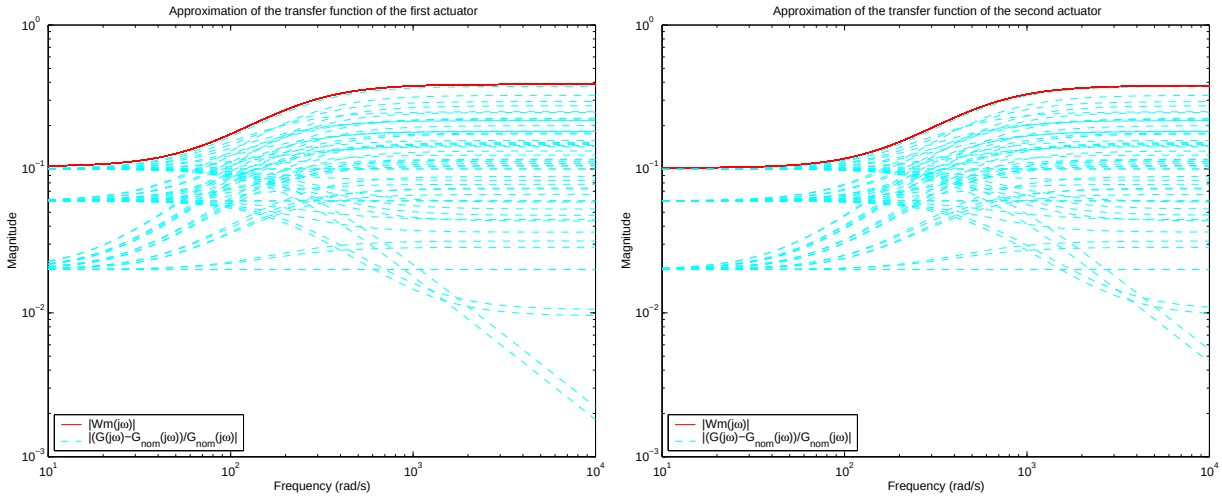


Figure 5: Actuators uncertainty approximation

by first order transfer functions. As a result one obtains

$$W_{m_1} = \frac{0.3877s + 25.6011}{1.0000s + 246.3606}, \quad W_{m_2} = \frac{0.3803s + 60.8973}{1.0000s + 599.5829}.$$

Let the inputs and outputs of $\delta_{m_1}$, $\delta_{m_2}$ are denoted by $y_{m_1}$, $y_{m_2}$ and $u_{m_1}$, $u_{m_2}$, respectively. Introducing the vectors $u = [u_1\ u_2]^T$, $u_m = [u_{m_1}\ u_{m_2}]^T$, $y_m = [y_{m_1}\ y_{m_2}]^T$ we obtain the actuators model

$$\begin{bmatrix} y_m \\ t_m \end{bmatrix} = G_m \begin{bmatrix} u_m \\ u \end{bmatrix}, \tag{3.4}$$

$$u_m = \Delta_m y_m \tag{3.5}$$

where

$$G_m = \begin{bmatrix} 0 & 0 & W_{m_1} & 0 \\ 0 & 0 & 0 & W_{m_2} \\ G_{m_1} & 0 & G_{m_1} & 0 \\ 0 & G_{m_2} & 0 & G_{m_2} \end{bmatrix}$$

and

$$\Delta_m = \begin{bmatrix} \delta_{m_1} & 0 \\ 0 & \delta_{m_2} \end{bmatrix}.$$

The uncertain behaviour of the actuators is described by the upper LFT

$$t_m = F_U(G_m, \Delta_m)u.$$

The overall tenth order, ten inputs and fourteen outputs model of the triple inverted pendulum system consisting of the pendulum and the actuators is shown in Figure 6. Note that $\Delta_m$ is a complex uncertainty while $\Delta_I$ and $\Delta_C$ are real uncertainties so that we have the case of mixed real and complex uncertainties.

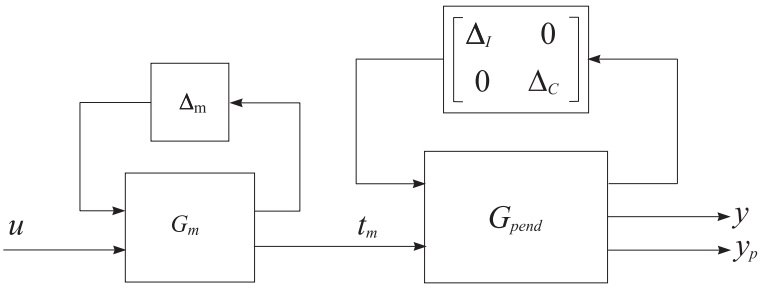


Figure 6: Triple inverted pendulum system with uncertainties

# 4 Closed-loop system performance requirements

The controller synthesis problem of the triple inverted pendulum system is to find a linear, output feedback, controller $K(s)$ which has to ensure the following properties of the closed-loop system.

**Nominal performance:** The closed-loop system achieves nominal performance if the performance objective is satisfied for the nominal plant model

$$\begin{bmatrix} y_m \\ y_I \\ y_C \\ y \\ y_p \end{bmatrix} = G_{nom} \begin{bmatrix} u_m \\ u_I \\ u_C \\ u \end{bmatrix}.$$

The transfer function matrix $G_{nom}$ is determined from the matrices $G_{pend}$ and $G_m$.

The performance objective is to satisfy the inequality

$$\left\| \begin{bmatrix} W_p S \\ W_u K S \end{bmatrix} \right\|_\infty < 1, \tag{4.1}$$

where $S = (I + G_{nom}K)^{-1}$ is the sensitivity function of the nominal system and $W_p$ and $W_u$ are chosen weighting functions. This objective corresponds to the mixed $S/KS$ sensitivity sub-optimization.

**Robust stability:** The closed-loop system achieves robust stability if the closed-loop system is internally stable for each possible plant dynamics $G = F_U(G_{nom}, \Delta)$ where

$$\Delta = \begin{bmatrix} \Delta_m & 0 & 0 \\ 0 & \Delta_I & 0 \\ 0 & 0 & \Delta_C \end{bmatrix}. \tag{4.2}$$

**Robust performance:** The closed-loop system must remain internally stable for each $G = F_U(G_{nom}, \Delta)$ and in addition the performance objective

$$\left\| \begin{bmatrix} W_p(I + GK)^{-1} \\ W_u K(I + GK)^{-1} \end{bmatrix} \right\|_\infty < 1 \tag{4.3}$$

should be satisfied for each $G = F_U(G_{nom}, \Delta)$.

In addition to those requirements it is desirable that the controller designed would have acceptable complexity, i.e. it is of reasonably low order.

The block diagram of the closed-loop system, which includes the feedback structure and the controller, as well as the elements reflecting the model uncertainty and the performance objectives, is shown in Figure 7. The rectangle, shown with dash line, represents the transfer function matrix $G$. Inside the rectangle is

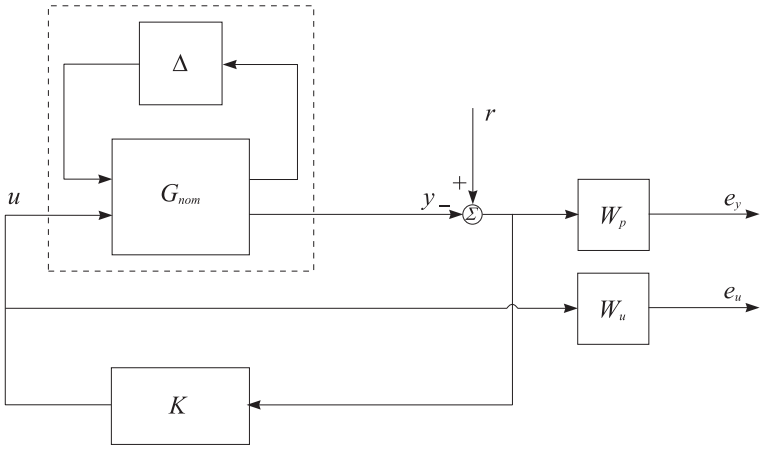


Figure 7: Closed-loop interconnection structure of the triple inverted pendulum system

the nominal model $G_{nom}$ of the triple inverted pendulum system and the block $\Delta$, which parametrizes the model uncertainties. The matrix $\Delta$ is unknown, but with the structure defined in (4.2) and with the norm bound $\|\Delta\|_\infty < 1$. The performance objective requires the transfer matrices from $r$ to $e_y$ and $e_u$ to be small in the sense of $\|.\|_\infty$, for all possible uncertain matrices $\Delta$. The transfer matrices $W_p$ and $W_u$ are used to reflect the relative significance of the different frequency ranges for which the performance is required.

According to the above considerations, the aim of the design is to determine a controller $K$, such that for all stable perturbations $\Delta$ with $\|\Delta\|_\infty < 1$, the perturbed closed-loop system remains stable and the perturbed weighted mixed sensitivity transfer function matrix to satisfy the condition

$$\left\| \begin{bmatrix} W_p(I + F_U(G_{nom}, \Delta)K)^{-1} \\ W_u K(I + F_U(G_{nom}, \Delta)K)^{-1} \end{bmatrix} \right\|_\infty < 1$$

for all such perturbations.

In the given case the weighting performance functions are chosen in the form

$$W_p(s) = \begin{bmatrix} w_p(s) & 0 & 0 \\ 0 & w_p(s) & 0 \\ 0 & 0 & w_p(s) \end{bmatrix}, \quad W_u(s) = \begin{bmatrix} w_u(s) & 0 \\ 0 & w_u(s) \end{bmatrix}$$

where

$$w_p(s) = 0.95\frac{s^4 + 12s^3 + 80s^2 + 80s + 65}{s^4 + 1500s^3 + 13000s^2 + 12000s + 65}, \quad w_u(s) = 0.006.$$

These weighting functions ensure an acceptable trade-off between the nominal performance and the robust performance of the closed-loop system.

## 5 $\mu$-synthesis and $D-K$-iterations

Let us denote by $P(s)$ the transfer function matrix of the thirteen inputs, sixteen outputs, open-loop system consisting of the pendulum system model plus the weighting functions and let the block structure $\Delta_P$ is defined as

$$\Delta_P := \left\{ \begin{bmatrix} \Delta & 0 \\ 0 & \Delta_F \end{bmatrix} : \Delta : 8 \times 8, \ with\ 6\ real\ and\ 2\ complex\ blocks\ ;\ \Delta_F \in \mathcal{C}^{3\times 5} \right\}.$$

The first block of this matrix corresponds to the uncertain block $\Delta$, used in modelling the uncertainty in the triple inverted pendulum system. The second block $\Delta_F$ is a fictitious uncertainty block, introduced to include the performance objectives in the framework of the $\mu$-approach. To meet the design objectives

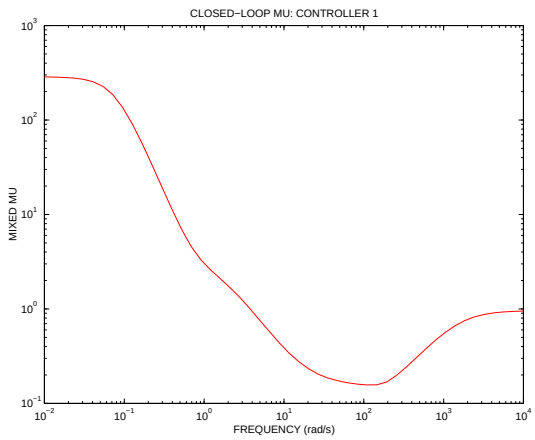


Figure 8: Frequency response of $\mu$ after the first D-K iteration

discussed in the last section, a stabilizing controller $K$ is to be found such that, at each frequency $\omega \in [0, \infty]$, the structured singular value [2] satisfies the condition

$$\mu_{\Delta_P}\left[F_L(P,K)(j\omega)\right] < 1.$$

The fulfillment of this condition guarantees robust performance of the closed-loop system, i.e.

$$\left\| \begin{bmatrix} W_p(I + F_U(G,\Delta)K)^{-1} \\ W_u K(I + F_U(G,\Delta)K)^{-1} \end{bmatrix} \right\|_\infty < 1$$

There have been several methods proposed so far to construct a $\mu$ controller, for instance, the $\mu$-$K$ iteration in [6]. In this work, however, the most popular method, the $D$-$K$ iteration, is to be applied. The details of the $D$-$K$ iteration method can be found in [3].

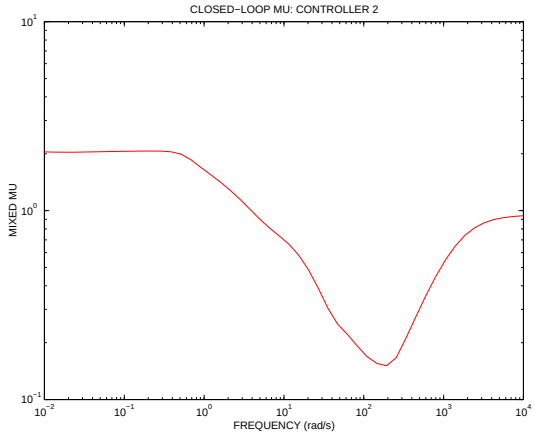


Figure 9: Frequency response of $\mu$ after the second D-K iteration

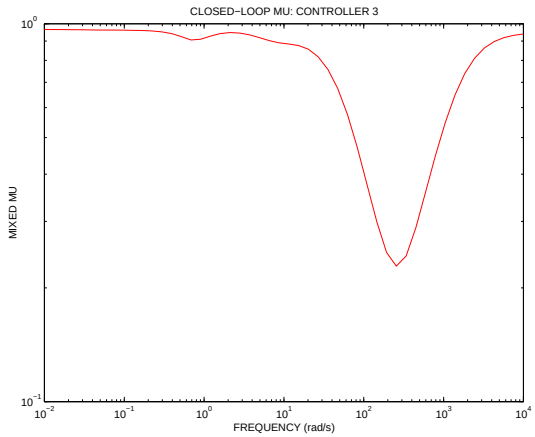


Figure 10: Frequency response of $\mu$ after the third D-K iteration

Table 3: Results of the $\mu$-synthesis

| Iteration | Controller order | Maximum value of $\mu$ |
|---|---|---|
| 1 | 25 | 127.8846 |
| 2 | 59 | 2.0609 |
| 3 | 71 | 0.96101 |

Here, the $\mu$-computation (the optimization over $D$ in the $D$-$K$ iteration) utilizes the mex-file `mucomp` based on the *SLICOT* routine `AB13MD`. In the triple inverted pendulum case, a satisfactory result is obtained

after three iterations. The frequency response plots of $\mu$ for each iteration is shown in Figures 8, 9 and 10, respectively. The order of the controllers along with the maximum values of $\mu$ in each iteration are shown in Table 3.

It can be seen from the table that after the third iteration the maximum value of $\mu$ is equal to 0.96101 which means that the robust performance has been achieved. The final controller obtained is of 71-st order.

# 6 $\mu$-controller analysis

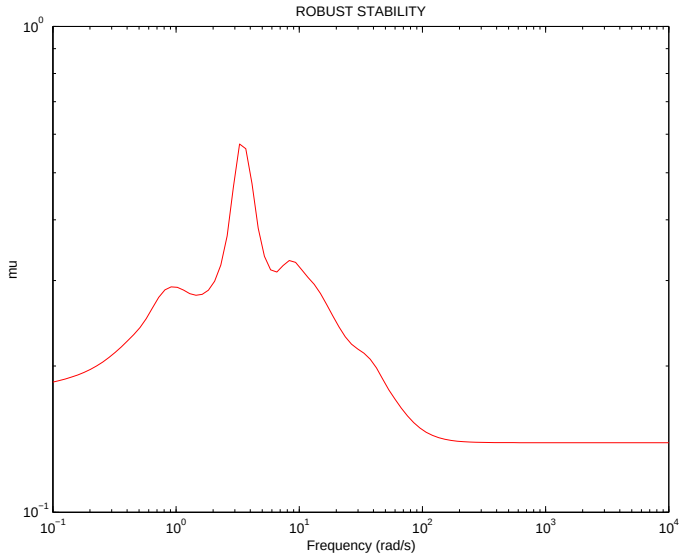


Figure 11: Robust stability of the closed-loop system with $\mu$-controller

The frequency response plot of the structured singular value for the case of robust stability is shown in Figure 11. The maximum value of $\mu$ is 0.57635 which means that the stability of the system is preserved under perturbations which satisfy $\|\Delta\|_\infty < \frac{1}{0.57635}$. In Figure 12 we show the individual contributions to $\mu$ due to the different types of uncertainties. It is seen that the uncertainty in the actuators has an influence in the low frequency range. While the uncertainties in the friction coefficients have larger effect also in the low frequency range, the uncertainties in the moments of inertia dominate in the high frequency range. The frequency responses of the nominal and robust performance are shown in Figures 13 and 14, respectively. The closed-loop system achieves robust performance since for arbitrary perturbations with unit norm it is fulfilled that

$$\left\| \begin{bmatrix} W_p(I + F_U(G,\Delta)K)^{-1} \\ W_u K(I + F_U(G,\Delta)K)^{-1} \end{bmatrix} \right\|_\infty < 0.96101.$$

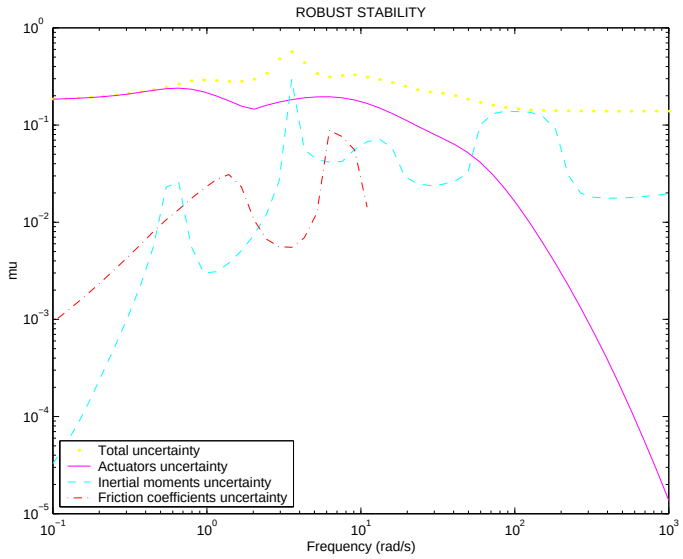


Figure 12: Contribution of the individual uncertainties to the robust stability of the closed-loop system with $\mu$-controller

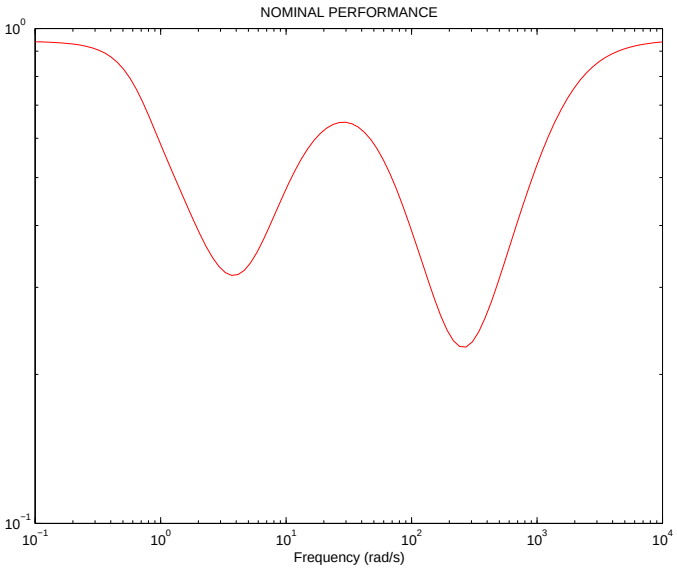


Figure 13: Nominal performance for the $\mu$-controller

# 7 Controller order reduction

As mentioned above, the controller obtained by $\mu$-synthesis is initially of 71-st order which makes the implementation in practice very difficult. Therefore, we have to consider to reduce the order of the controller.

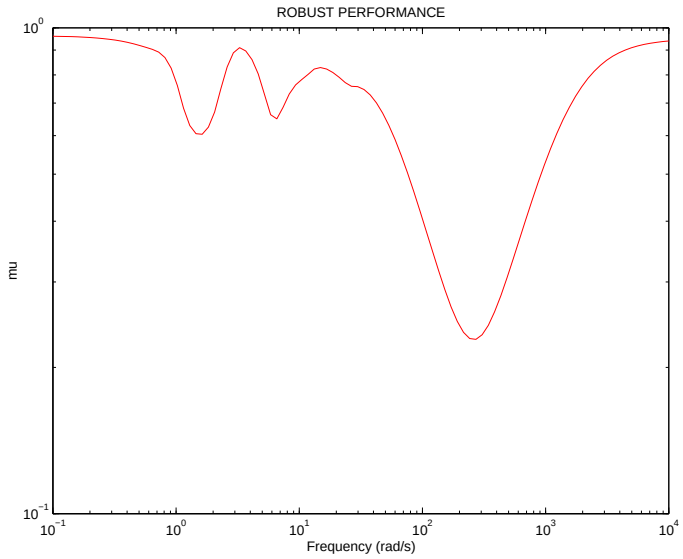


Figure 14: Robust performance for the $\mu$-controller

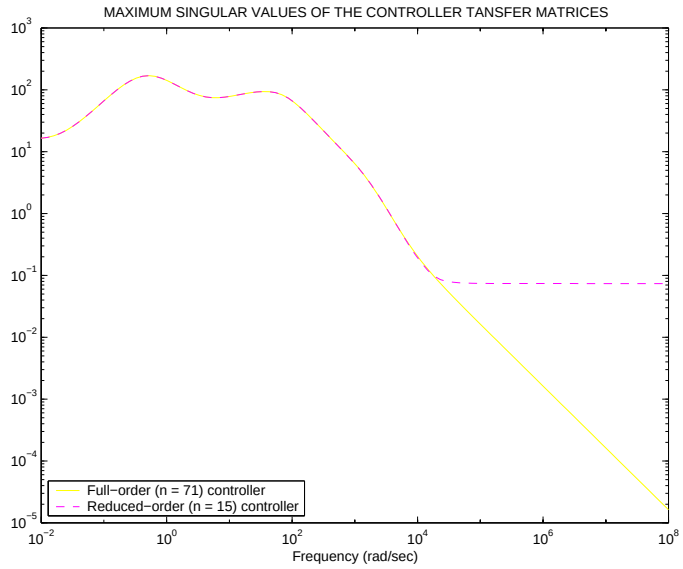


Figure 15: Frequency responses of the full order and reduced order controllers

The mex-file `sysred` which implements several *SLICOT* model reduction routines is applied. In the present case we use system balancing followed by optimal Hankel approximation which allows to reduce the controller order to 15. Further reduction of the controller order leads to deterioration of the closed-loop transient responses and even to instability.

In Figure 15 we compare the frequency responses of the maximum singular values of the full order and reduced order controllers. Up to the frequency $10^4 rad/s$ the frequency plots of both controllers coincide which implies similar performance in the closed-loop system. In particular, the transient responses of the

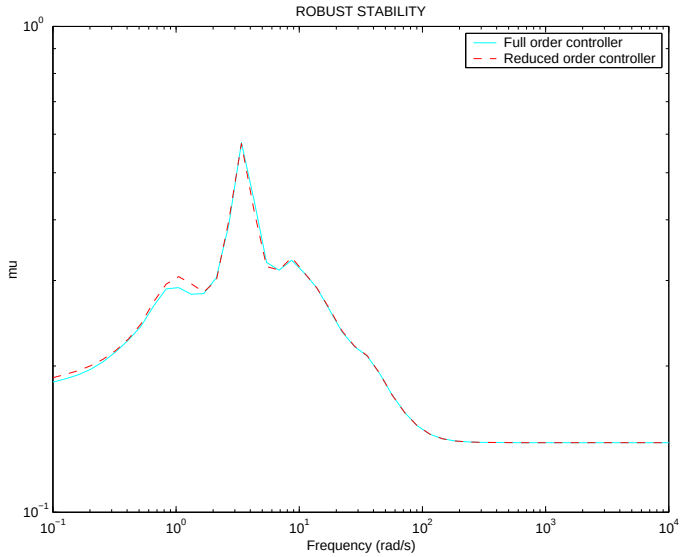


Figure 16: Comparison of the robust stability for full order and reduced order controllers

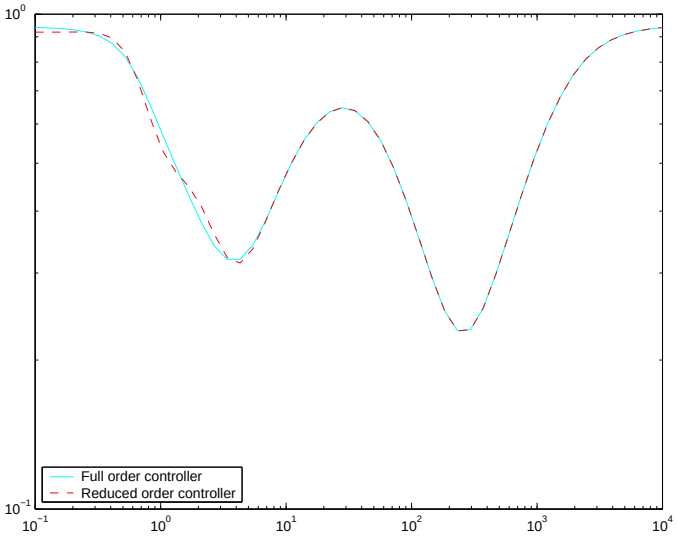


Figure 17: Comparison of the nominal performance for full order and reduced order controllers

closed-loop system with full order and with the reduced order controller are practically undistinguishable.

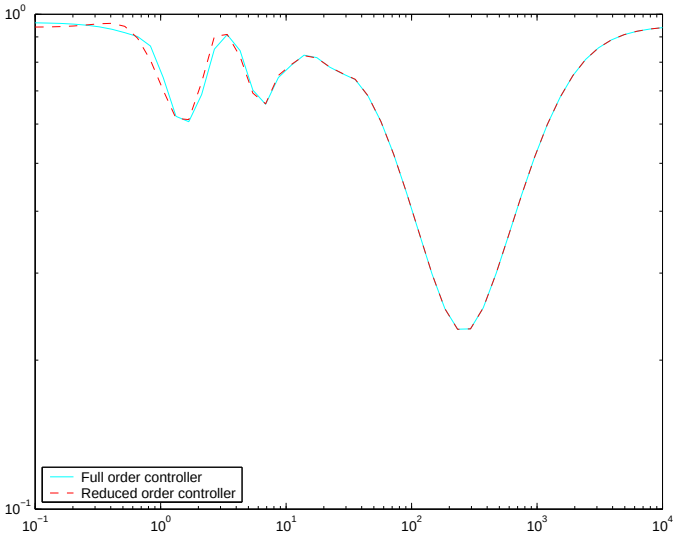


Figure 18: Comparison of the robust performance for full order and reduced order controllers

In Figures 16, 17 and 18 we compare the robust stability, nominal performance and robust performance, respectively, for the full order and reduced order controllers in terms of frequency response criteria. It is clear from the figures that both controllers produce almost identical results.

# 8 Closed-loop system simulations

In Figure 19 we show the transient response of the closed-loop system with $\mu$-controller for initial condition

$$\Theta_1 = 0,\ \Theta_2 = 0,\ \Theta_3 = 0.02\ rad,$$

and in Figure 20 we show the transient response for reference

$$r_1 = 0,\ r_2 = 0,\ r_3 = 0.02\ rad.$$

In both simulations, the reduced order $\mu$ controller was used. It can be seen that the closed-loop system performed satisfactorily in both cases.

In Figures 21, 22 we show the respective transient responses of the third output for a family of perturbed closed-loop systems, with the reduced order controller, obtained for different real parameters satisfying $-1 \leq \delta_{I_i}, \delta_{C_i} \leq 1, \quad i = 1,2,3$ and zero complex parameters $\delta_{m_i}, \quad i = 1,2$. In both cases the perturbed transient responses are close to the corresponding nominal transient responses and are satisfactory.

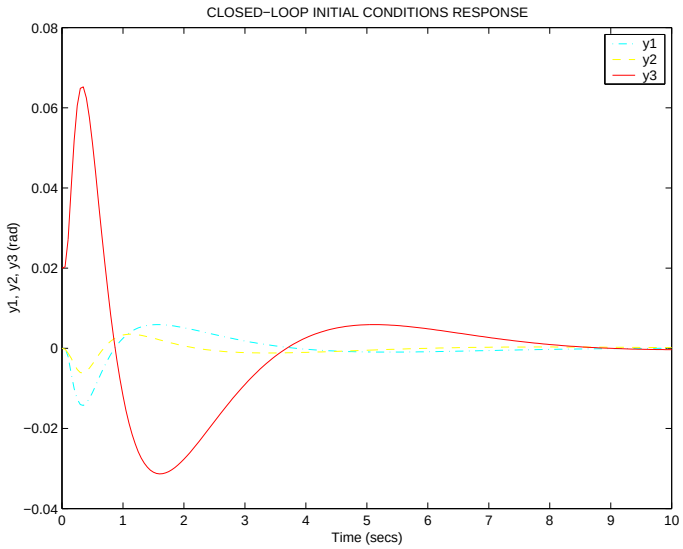


Figure 19: Closed-loop initial conditions transient response for the $\mu$-controller

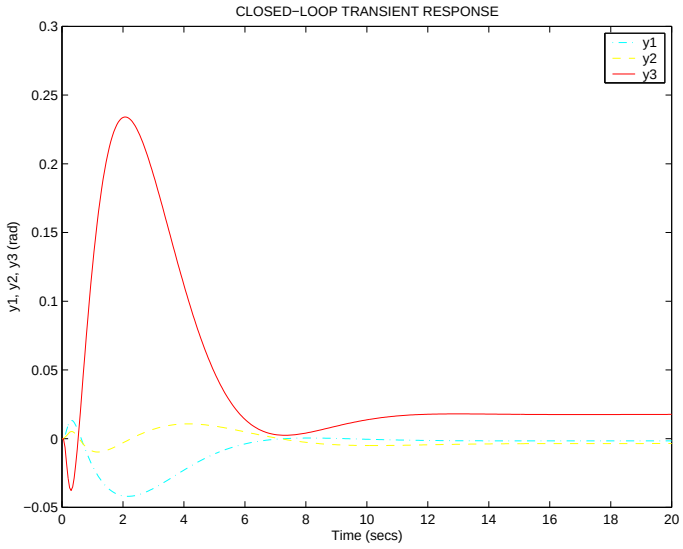


Figure 20: Closed-loop reference transient response for the $\mu$-controller

# 9 Conclusions

In this report, the design of a robust controller for a triple inverted pendulum system using the $\mu$-synthesis approach was presented. The designed controller meets all the objectives including robust stability and robust performance requirements. Further, a model reduction procedure was applied to the $\mu$-controller,

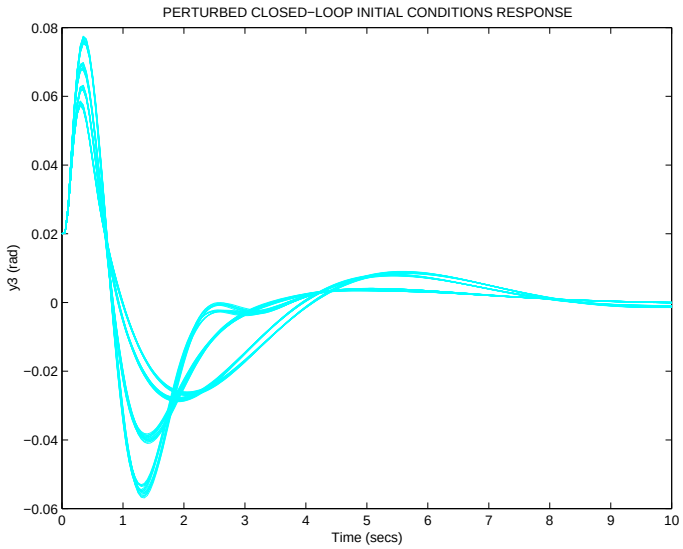


Figure 21: Perturbed closed-loop initial conditions transient responses

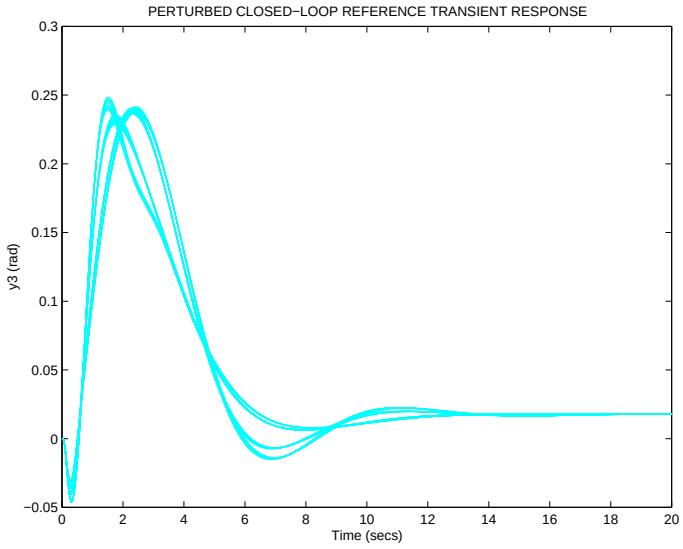


Figure 22: Perturbed closed-loop reference transient responses

which reduced the order of the controller from 71 to 15. Closed-loop system responses with the reduced order controller show satisfactory results.

In the design, the structured singular value $\mu$ was calculated with the *SLICOT* routine `AB13MD` and the model reduction toolbox in *SLICOT* was used in reducing the order of the $\mu$ controller. The computation experience shows that the *SLICOT* routines perform better than the counterpart routines in *MATLAB* in

terms of speed and accuracy.

# References


[1] G.J. Balas, J.C. Doyle, K. Glover, A. Packard and R. Smith. *$\mu$-Analysis and Synthesis Toolbox*, The MathWorks Inc., 1998.

[2] J.C. Doyle. *Analysis of feedback systems with structured uncertainties. IEE Proceedings*, Part D, **vol.133**, pp. 45-56, 1982.

[3] J.C. Doyle, K. Lenz and A. Packard. *Design Examples using $\mu$ Synthesis: Space Shuttle Lateral Axis FCS during Reentry. IEEE CDC Proceedings*, pp. 2218-2223, December 1986.

[4] K. Furuta, K. Kajiwara and K. Kosuge. *Digital control of a double inverted pendulum on an inclined rail. Int. J. Control*, **vol. 32**, pp. 907-924, 1984.

[5] K. Furuta, T. Ochia and N. Ono. *Attitude control of a triple inverted pendulum. Int. J. Control*, **vol. 39**, pp. 1351-1365, 1984.

[6] J.-L. Lin, I. Postlethwaite and D.-W. Gu. *$\mu$-K Iteration: A New Algorithm for $\mu$-synthesis. Automatica*, **vol.29, No. 1**, pp. 219-224, 1993.

[7] G.A. Medrano-Cerda. *Robust stabilization of a triple inverted pendulum-cart. Int. J. Control*, **vol. 68**, pp. 849-865, 1997.

[8] Z. Meier, H. Farwig, H. Unbehauen. *Discrete computer control of a triple-inverted pendulum*, *Optimal Contr. Appl. & Meth.*, **vol. 11**, pp. 157-171, 1990.

[9] V.A. Tsacouridis, G.A. Medrano-Cerda. *Discrete-time $H_\infty$ control of a triple inverted pendulum with single control input. IEE Proc.-Control Theory Appl.*, **vol. 146**, pp. 567-577, 1999.

[10] K. Zhou, J.C. Doyle and K. Glover. *Robust and Optimal Control*, Prentice Hall, Upper Saddle River, N.J., 1996.